In vitro cellular biocompatibility and *in vivo* degradation behavior of calcium phosphate-coated ZK60 magnesium alloy

Le Thi Trang[a], Le Van Hai[b], Sachiko Hiromoto[c], Minho O[a], Equo Kobayashi[a,*], Nguyen Viet Nam[d], Nguyen Quang Cao[e]

[a] *Department of Materials Science and Engineering, Tokyo Institute of Technology, 2-12-1 Ookayama, Meguro, Tokyo, 152-8550 Japan*

[b] *103 Military Hospital, Vietnam Military Medical University, 160, Phung Hung, Phuc La, Ha Dong, Hanoi, Vietnam*

[c] *Research Center for Structural Materials, National Institute for Materials Science, 1-2-1 Sengen, Tsukuba, Ibaraki, 305-0047 Japan*

[d] *Institute of Traumatology and Orthopedics, 108 Military Central Hospital, 1B Tran Hung Dao, Bach Dang, Hai Ba Trung, Hanoi, Vietnam*

[e] *Laboratory for Biomaterials and Bioengineering, Université Laval, 2325 Quebec, G1V 0A6 Canada*

*Corresponding author**:** Equo Kobayashi*

Email: equo@mtl.titech.ac.jp / Fax number: 03-5734-3147

Address: S8-18, 2-12-1 Ookayama, Meguro City, Tokyo 152-8550

Abstract:

Calcium phosphate (Ca-P) surface coating is a simple but effective way to enhance both corrosion resistance and biocompatibility of ZK60 magnesium alloy. However, cell compatibility on different Ca-P layers coated on ZK60 alloy has seldom been investigated. In this study, the effects of type, morphology and corrosion protection of several Ca-P coatings formed at pH 6.5, 7.8 and 10.2 on cell behavior were examined by using an osteoblastic cell line MC3T3-E1. Furthermore, i*n vivo* behavior in rabbits of the alloy coated with the optimum Ca-P layer was also studied. It was found that the surface factors governed the cell morphology and density. The coating morphology plays a dominant role in these surface factors. The sample coated at pH 7.8 showed the best cellular biocompatibility, suggesting that the hydroxyapatite (HAp) layer formed at pH 7.8 was the optimum coating. In rabbits, this optimum coating enhanced remarkably the corrosion resistance of the alloy. During implantation, the outermost crystals of the HAp coating were shortened and thinned due to the dissolution of HAp caused by the body fluid of the rabbits. It is indicated that ZK60 alloy coated at pH 7.8 can be applied as a biodegradable implant.

Key words: ZK60, calcium phosphate coating, cellular biocompatibility, biodegradation, implantation

1. Introduction

In recent years, magnesium (Mg) alloys have evolved as potential materials for biodegradable implant devices due to their outstanding properties, including their comparable density and elastic modulus to those of human bones, biocompatibility and biodegradability [1], [2]. In biomedical use, the biosafety of the alloying elements contained in a particular Mg alloy system should also be taken into consideration. In Mg-6mass% Zn-0.5mass% Zr (ZK60) alloy, both Zn and Zr alloying elements with the designated amount are proved to be biocompatible [3], [4]. The addition of Zn and Zr leads to the solid solution hardening effect and the grain-size strengthening effect for the alloy, respectively [3], [5], which enhance the mechanical properties to meet the requirement of load-bearing applications [6]. However, the low corrosion resistance of ZK60 alloy causes concern for clinical use such as hydrogen gas evolution, local alkalization, loosening of mechanical integrity or the fracture of the implant [7], [8], [9].

To improve the corrosion resistance and enhance the biocompatibility of Mg/Mg alloys, surface treatment with calcium phosphate (Ca-P) coatings is extensively studied because Ca-P compounds are minerals found in hard human tissues and have low solubility [10]. In addition, modified Ca-P coatings exhibited good antibacterial performance, which could avoid serious biofilm-associated infections caused by bacteria [11], [12], [13], [14]. The Ca-P coatings also showed good bioactivity because their surface contains negatively charged functional groups which strongly induce biomineralization of Ca-P crystallites on the implant by electrostatically interacting with the calcium and phosphate ions in the body fluid [15]. Among various coating methods, the chemical conversion method introduced by Hiromoto et al. is a simple and cost-effective single-step process using environmentally friendly reagents and can apply to any shape of the device [16]. The Ca-P coating can be in the form of octacalcium phosphate (OCP, $Ca_8(PO_4)_4(HPO_4)_2.5H_2O$) with its specific plate-shaped crystals, or hydroxyapatite (HAp, $Ca_{10}(PO_4)_6(OH)_2$) with rod-/needle-shaped crystals [17]. Numerous studies proved that cell behavior on a Ca-P-coated material depends strongly on the type, morphology and corrosion property of the coating [18], [19], [20], [21]. It is reported that the corrosion property of different types of the Mg-based alloy substrate influenced the morphology and corrosion protectiveness of the Ca-P coating deposited in the chemical conversion method [22], [23]. In our previous study, we investigated the formation and corrosion behavior of different Ca-P coatings formed on ZK60 alloy [24]. The type, morphology and corrosion protectiveness of the formed coatings varied at different pH coating conditions. However, the influence on cellular biocompatibility of the Ca-P coatings with different surface properties formed on ZK60 alloy have not been investigated yet.

Therefore, in this work, the cell viability of those Ca-P coatings formed at pH 6.5, 7.8 and 10.2 on ZK60 alloy was investigated. Furthermore, animal tests were carried out in rabbits to provide a comprehensive view of the *in vivo* degradation behavior of ZK60 alloy that uncoated and coated with the optimum Ca-P coating to determine the feasibility of use.

2. Materials and Methods

2.1. Material preparation

In this study, commercially as-extruded ZK60 alloy samples (5.28wt% Zn, 0.521wt% Zr, 0.0032wt% Al, 0.006wt% Mn, 0.0006wt% Fe, 0.0025wt% Si, 0.0007wt% Cu, 0.0006wt% Ni, Mg Bal., Osaka Fuji Industry, Japan) with 20 mm in diameter and 2 mm in thickness were used as a substrate. The samples were ground mechanically by SiC abrasive papers from 500 grits to 4000 grits, cleaned with ethanol and then dried in air. Different calcium phosphate coating layers were formed on the surface of the substrate by the chemical conversion method [16]. The coating solution was prepared by mixing 0.5 mol/L ethylenediaminetetraacetic acid calcium disodium salt hydrate ($C_{10}H_{12}CaN_2Na_2O_8.xH_2O$, Ca-EDTA) solution and 0.5 mol/L potassium dihydrogen phosphate (KH_2PO_4) solution. The pH value of the coating solution was adjusted to 6.5, 7.8 and 10.2 by adding 1 mol/L NaOH solution. The samples were coated at a stable temperature of 90^0C for 2 h. Both the uncoated and coated samples were dehydrated and kept in a vacuum environment for further investigation. The crystal phase of the calcium phosphate coatings was characterized by an X-ray diffractometry (XRD; Rigaku, RINT-Ultima III) using Cu-K_α radiation (λ=0.154184 nm) generated at 30 kV and 10mA. The XRD patterns of the samples were obtained with a scan step of 0.02^0 and 0.5s per step. A field-emission scanning electron microscope (FE-SEM; JSM-7200F, JEOL) equipped with an energy dispersion X-ray spectrometer (EDS) was used to analyze the surface and cross-sectional morphology of the calcium phosphate coatings.

2.2. In vitro cell culture tests

To examine the *in vitro* biocompatibility of the samples coated at different pH conditions, initially, osteoblastic MC3T3-E1 cells (RIKEN Cell Bank) were prepared through thawing and passaged 4 to 5 times. A α-minimum essential medium (α-MEM) supplemented with 10% fetal bovine serum and 1% penicillin/streptomycin solution was used as a culture medium. Before cell seeding, the uncoated and coated samples were sterilized in acetone, then placed in the 12-well plates. The cells were seeded on the samples at a density of 2×10^4 cells/cm^2 in 3 ml of the culture medium in each well and incubated at 37^0C with 5% CO_2 for 24 h and 72 h. The cells were also seeded in 12-well plates which is made by polystyrene, functioning as negative control groups. Each type of the samples and the negative control groups were

triplicated in the culture test. After the incubation, the cells were fixed on the surface of the samples by methanol and stained by Giemsa solution for cell counting and observation. After this staining process, the samples were cleaned by the purified water, dried completely and kept in a vacuum environment for further investigation. To calculate the cell density, five regions with the same area on the surface of the cultured samples, as illustrated in figure 1, were captured by optical microscope (OM, VHX-5000, Keyence). The number of cells in each region was counted by using ImageJ software. The average cell densities were compared using a one-way analysis of variance (ANOVA). A post hoc test with Bonferroni correction was employed to analyze significant differences between samples. Additionally, the pH value of the culture medium was also measured. Mg ion concentration was quantified by a colorimetric method using xylidyl blue-I [25], [26] using a test kit, Magnesium B-test Wako (FUJIFILM Wako, Japan). The absorption wavelength of the chelate of xylidyl blue-I and Mg ions at 520nm was measured by a microplate spectrophotometer (Thermo Scientific, Multiskan Go). The cell morphology and *in vitro* corrosion on the cultured samples were observed by a FE-SEM equipped with an EDS. The ImageJ software was used to measure the nucleus area of the randomly selected cells (n=30) on each type of the samples.

2.3. In vivo subcutaneous implantation test in rabbits

The animal experiments were approved by the Science Council of Vietnam Military Medical University, Ministry of National Defense, Hanoi, Vietnam (No. 838/QD-HVQY) and performed at the Animal Center of Vietnam Military Medical University, Ministry of National Defense, Hanoi, Vietnam. The animal (rabbits) were cared according to “Guidelines on Experimental Food or Water Restriction or Manipulation in Laboratory Animals” proposed by University of Michigan, Michigan, America.

The samples uncoated and coated at pH 7.8 were used for the implantation tests. A total of 8 healthy and domestic white rabbits of about 2-2.5kg in weight and 6-8 months in age were housed in separate cages under controlled living and feeding conditions. The rabbits were randomly divided into two groups, each containing 4 individuals who were employed for one type of samples. Before the surgery, the rabbits were anesthetized with propofol (15-25 mg/kg/h). One side of the hindquarter knees of the rabbits was shaved, then disinfected with betadine 10% solution. The skin and subcutaneous tissue were opened carefully layer after layer. The samples were placed in the hindquarter knee muscle. One sample was implanted in one rabbit. The subcutaneous tissue was closed by an absorbable bio-suture, while the skin was closed by a nonabsorbable bio-suture. After the wound was closed, the surgical sites were disinfected again with the betadine 10% solution. The rabbits were then returned to their cages. They were looked after carefully and periodically after the surgery. At either the fourth week or twelfth week post-implantation, a secondary surgery was performed to retrieve the samples from the rabbits. Before the secondary surgery, the implanted

position on each rabbit was scanned by X-ray radiography (Siemens 100, Germany). The retrieved samples were dried in air, kept under a vacuum condition and characterized by OM, FE-SEM and EDS.

3. Results

3.1. Coating results

Figure 2 shows the X-ray diffraction patterns of the uncoated and coated samples [24]. The sample coated at pH 6.5 showed the characteristic peak from $(010)_{OCP}$ at 4.7^0 (diffraction file of OCP No. 44-0778), indicating the formation of OCP. On the other hand, the sample coated at pH 7.8 and 10.2 showed the characteristic peak from $(002)_{HAp}$ at 26.0^0 (diffraction file of HAp No. 00-009-0432), indicating the formation of HAp. Furthermore, the diffraction peak at 18.5^0 from $(001)_{Mg(OH)2}$ was observed at pH 10.2 (diffraction file of $Mg(OH)_2$ No. 7-239), suggesting that $Mg(OH)_2$ was formed with HAp. It is previously reported that $Mg(OH)_2$ formed as an intermediate layer between the HAp coating and the substrate [24], [27].

Figure 3 exhibits the structure and morphology of the calcium phosphate coatings formed at pH 6.5, 7.8 and 10.2 [24]. The pH 6.5 coating has a 1.0 μm inner layer and a porous outer layer containing plate-shaped OCP crystals with a length from 0.9 to 3.6 μm. In comparison, the HAp coatings formed at pH 7.8 and 10.2 have a thicker inner layer and more frequent distribution of the outermost crystals. Rod-shaped HAp crystals with a length of 3.0 μm were observed at pH 7.8, whereas agglomerates of needle-shaped HAp crystals with a length of 1.4 μm were observed at pH 10.2. The needle-shaped crystals of HAp were depicted to have a diameter of several tens of nanometers with a very sharp tip [17]. Moreover, on the surface of the pH 10.2 coating, cracks and displacement among the agglomerates were observed, which were highlighted by black arrows.

3.2. Cell viability and in vitro corrosion behavior of different types of samples

Figure 4 shows the whole surface OM images of the samples with and without calcium phosphate coatings cultured with MC3T3-E1 cells retrieved after 24h and 72h. Figure 5 indicates the average cell density that counted on the corresponding samples in figure 4 after the cell culture test. After 24h, the cell density on the uncoated sample showed no statistically significant difference with either the seeding density or the density of the negative control group. However, no cells were observed after 72h. The cell densities of the samples coated at pH 6.5 and 7.8 were comparable to each other, but both were significantly higher than the seeding density approximately 50% and 100% after 24h and 72h, respectively. Compared with the negative control group, the cell densities on these two samples showed negligible difference after 24h but were about twice lower after 72h. Nevertheless, a decreasing trend of the cell density was observed in the

sample coated at pH 10.2. Only about 26.4% of the seeded cells remained on this sample after 72h. The results indicate that the sample coated at pH 6.5 and 7.8 showed a better condition for cell adhesion and proliferation.

Figure 6 (a) to (p) reveal the morphology of the cells that adhered to the samples after 24h and 72h of the cell culture. On the uncoated sample, the cells showed a small nucleus after 24h but no cells were observed after 72h owning to the covered layer of crystallized corrosion products. On the sample coated at pH 10.2, a shrinkage of the cell body was observed since 24h of the culture test, shown in the cell extension and small nucleus. After 72h, the cells shrunk severely. On the other hand, the cells which adhered on the sample coated at pH 6.5 and 7.8 manifested elongated morphology and a large nucleus after 24h and 72h, suggesting better cell morphology [28]. Figure 6 (q) depicts that the average nucleus area of the cells on the sample coated at pH 7.8 is larger than that of the cells on the sample coated at pH 6.5 after either 24h or 72h. It demonstrates that the sample coated at pH 7.8 has a more suitable surface for the osteoblastic cells than that coated at pH 6.5 [28].

In vitro corrosion morphology of the cultured samples after 24h and 72h is demonstrated in figure 7. After 24h, localized corrosion was observed on the uncoated sample with microcracks, shown in figure 7 (a). In figure 7 (i), dark grey regions of corrosion product of $Mg(OH)_2$ and pits with a depth of 1.9-2.7 μm were observed underneath the surface. After 72h, the uncoated sample was covered by a layer of corrosion products with a thickness of 3.8-12.1 μm, shown in figure 7 (e) and (m). Localized corrosion was observed on the surface of the samples coated at pH 6.5, in figure 7 (b) and (f), and at pH 7.8, in figure 7 (c) and (g), both after 24 h and 72 h. A thin layer of $Mg(OH)_2$ corrosion product was more clearly observed in the cross-section of the sample coated at pH 6.5, in figure 7 (j) and (n), than that of the sample coated at pH 7.8 in figure 7 (k) and (o). In the case of the sample coated at pH 10.2, filiform corrosion occurred with the formation of the corrosion product of $Mg(OH)_2$ underneath the coating after 24h and 72h. This localized corrosion detached the coating from the substrate, which caused various cracks in a high vacuum environment during SEM observation, shown in figure 7 (d) and (h).

Figure 8 demonstrates the pH change of the culture medium for each type of the sample after two culture intervals. After 24 h, the pH value of the medium for the samples coated at pH 6.5 and 7.8 slightly increased to 7.7 and 7.6, respectively. Meanwhile, the pH value of the medium for the samples that was uncoated and coated at pH 10.2 increased notably to 8.2 and 8.1, respectively. After 72 h, the medium for all the samples showed a significant increase in the pH value, compared to the original pH value (pH = 7.4). The highest increase was observed for the sample coated at pH 10.2, to 8.9, whereas the lowest increase was observed for the sample coated at pH 7.8, to 8.3.

Figure 9 depicts the Mg^{2+} ion concentration released into the culture medium owing to the corrosion of the samples. After 24h, the released amount of the Mg^{2+} ions from the samples coated at pH 6.5 and 7.8 was comparable and approximately triple lower than the released amount from the two other samples. However, the released amount from the samples coated at pH 6.5 and 7.8 showed a great increase after 72h, to 7.9×10^{-2} and 6.2×10^{-2} mg/cm^2, respectively. Nonetheless, the released amount from the uncoated sample and the sample coated at pH 10.2 raised slightly, to about 10.1×10^{-2} mg/cm^2.

3.3. Performance of subcutaneously implanted samples in rabbits

Figure 10 (a) to (d) demonstrates radiographic images of the rabbits implanted with the uncoated and coated samples at two different periods post-surgery. At four weeks post-surgery, both kinds of the implanted samples showed a large volume of gas around the sample (figure 10 (a) and (b)). The formation of gas cavities around the implanted samples indicates the occurrence of encapsulation of the samples during implantation. Figure 10 (e) shows the subcutaneous appearance of the implantation site of the uncoated sample at four weeks post-surgery as an example. The gas cavity formation was observed to cause a local swelling of the host tissue surrounding the implantation site. At twelve weeks post-surgery, a large volume of gas entrapped in the capsule was still observed around the uncoated sample (figure 10 (c)), whereas the gas volume reduced significantly around the coated sample (figure 10 (d)).

Figure 11 shows microscopy images of the samples implanted in the rabbits for different implantation periods. Since the samples were retrieved without cleaning, the trace of the blood and surrounding soft tissue that adhered tightly to the samples was obviously seen, especially after twelve weeks of implantation, shown in figure 11 (c) and (d). After four weeks, the surface of the uncoated sample was observed with some severely corroded regions. On the coated sample, large cracks were visibly observed, pointed out by white arrows. The HAp coating was partly collapsed, in which the remaining region of the coating is in white color, and the collapsed region is in dark color. After twelve weeks, not only the surface but also the edge of the uncoated sample was corroded severely, leading to an irregular shape of the sample. Nonetheless, the coated sample was covered by an inhomogeneous layer. The shape of this sample was kept as the original. The results indicate that the coated sample showed higher corrosion resistance than the uncoated sample.

Figure 12 shows the surface and cross-sectional corrosion morphology of the implanted samples. Figure 12 (a-1) and (a-2) correspond to the areas 1 and 2 on the sample shown in figure 11 (a). Other surface images (b-1) to (d-2) are also in the same manner. The images (e-1) to (h-2) are the cross-sectional view of the areas 1 and 2 on the samples (a) to (d) also in figure 11. EDS analyses were carried out on the white frame in the (c-1) to (d-2). For the uncoated sample, there was a highly rough layer of corrosion products

in the area 1, whereas the area 2 had a flat surface with numerous cracks. The observed cracks may be caused by the high vacuum condition during SEM observation. For the coated sample, a part of the coating was collapsed at four weeks post-surgery, while localized corrosion was observed on the remaining coating layer, in figure 12 (b-1) and (b-2). At twelve weeks post-surgery, this sample was covered by a layer of corrosion products with no observation of the coating, in figure 12 (d-1) and (d-2).

In the cross-section observation, for the uncoated sample, pits with a depth from 90 to 125μm were observed during implantation, shown in figure 12 (e-1) and (g-1). On the other hand, even though pitting corrosion was also observed for the coated sample, the pits were shallower with a depth less than 75μm, in figure 12 (f-1) and (h-1). It indicates a higher corrosion resistance of the coated sample. At twelve weeks post-surgery, a corrosion product layer with a thickness of about 11μm was covered the coating layer, in figure 12 (h-2).

By EDS analysis, the corrosion products containing mainly Mg, Ca, P and O deposited on the surface of the samples, indicating the deposition of Ca/Mg inorganic salts. The high concentration of C might be from soft tissue, protein, amino acid, etc., in the rabbits. The presence of Al element was considered as a contamination because of the use of aluminum tweezer and container during the surgeries. Additionally, $Mg(OH)_2$ corrosion product was found mainly in the pitting area. The formation of $Mg(OH)_2$ underneath the HAp coating layer indicates the penetration of the body fluid through the coating, which led to the corrosion of the ZK60 alloy, in figure 12 (f-2) and (h-2). Regarding to the composition of the corrosion product layer in figure 12 (h-2), it is reported that in the corrosion product layer formed under the activities of macrophages, which is the main cause of *in vivo* corrosion, the outer part contained mainly Ca/Mg salts while the inner part contained mainly $Mg(OH)_2$ [29]. It shows an agreement with the EDS analysis on the surface and cross section in this study, in which the surface of the layer contained Mg, Ca, O, P and C (figure 12 (d-2)) while $Mg(OH)_2$ presented mainly in the inner part of this layer (figure 12 (h-2)).

Figure 13 shows the change of the HAp coating formed at pH 7.8 after implantation. The initial distribution of the HAp crystals was frequent, shown in figure 13 (a), whereas the latter distribution became more sparsely after four weeks of implantation, as in figure 13 (b). Additionally, the HAp crystals in the outermost layer were thinned and shorten, as in figure 13 (b), (d) and (e), compared with the original crystals in figure 13 (a) and (c). It depicts that the HAp coating was dissolved by the body fluid of the rabbits during implantation. After twelve weeks of implantation, there was no notable change of the coating. It is attributed to the protection of the corrosion product layer covered the coating.

4. Discussion

4.1. Cell viability and in vitro corrosion behavior of different calcium-phosphate coated samples

It is stated that the cells do not contact directly on the bare surface of a material, but on the surface that previously was adsorbed by water or proteins from the cell culture medium [20]. The cells adhere to the surface of the biomaterial by forming focal contacts based on the adsorbed layer, then spread out, proliferate and eventually differentiate. Therefore, the adsorbed protein layer plays an essential role in the cell response to the biomaterials. In the case of the uncoated samples, the cell density showed no statistically significant difference with the seeding density and the density of the negative control group after 24h (figure 5) even though the sample was corroded to some extent, shown in figure 7 (a) and (i). This is because (1) the proteins in the culture medium inhibit the initial corrosion of ZK60 alloy by the discontinuously adsorbed layer and the formation of an insoluble salt layer acts as a local corrosion barrier [30], (2) the abundant amount of Mg ions due to Mg corrosion can result in rapid protein adsorption [30] and (3) Mg ions promote the cells to synthesize protein and DNA and then proliferate [31]. However, it is noted that the cell nucleus was much smaller than the nucleus of the cells adhered to the coated samples, as in figure 6 (e). After 72h, no cells survived on the uncoated sample, shown in figure 5. This is attributed to the fast degradation of ZK60 alloy since the adsorbed protein layer is discontinuous, leading to a drastic pH increase in figure 8, hydrogen gas evolution and the formation of a thick layer of corrosion products, as in figure 7 (e) and (m). Those events limited the cell adhesion, consequently caused the cell death [32], [33].

In contrast, the ZK60 samples covered by the calcium phosphate coatings showed good *in vitro* biocompatibility because organic macromolecules, such as amino acids and proteins, have a high affinity for calcium phosphate apatite surface due to the active Ca and P sites [34] [35] [36], leading to a notable increase in the adsorbed protein layer. The outer layer of the coatings exhibited high micro-sized porosity, as in figure 3, which also benefits for the protein absorption [21]. Hence, the coated samples provided a favorable surface for cell adhesion and then proliferation. Additionally, the calcium phosphate coatings also delayed the occurrence of corrosion, shown in figure 8 and 9. Therefore, the samples coated at pH 6.5 and 7.8 showed good biocompatibility with a remarkable increase in the average cell density and the extension of the cell body on their surface. However, the cells manifested more elongated shape, which characterizes for the osteoblastic cell line, and a larger nucleus on the sample coated at pH 7.8, as in figure 6 (q) although the average cell density showed no statistical significance between the two samples. This is because the formation of focal contacts of the pre-osteoblasts on the rod-shaped HAp crystals of the pH 7.8 coating was better than on the plate-shaped OCP crystals of the pH 6.5 coating [33]. In addition, the sample coated at pH 7.8 was less corroded than that coated at pH 6.5, shown in figures 7, 8 and 9 because of both the lower solubility [37] and a thinner inner layer of the OCP coating compared to those of the HAp coating,

shown in figure 3 (g) and (h). Therefore, the sample coated at pH 7.8 provided a preferential surface for cell adhesion and growth.

However, the sample coated at pH 10.2 showed low biocompatibility for the osteoblastic cells, although the sample was coated with a HAp layer. The average cell density showed a decreasing trend in figure 5 and the cells shrunk severely after 72h in figure 6 (p). In our previous study, the induction time for corrosion initiation of this sample is much shorter than the sample coated at pH 6.5 and 7.8 but longer than the uncoated sample [24]. This fast occurrence of filiform corrosion caused the low biocompatibility for the sample coated at pH 10.2. The filiform corrosion caused the formation of large regions of the corrosion product of $Mg(OH)_2$ underneath the coating, in figure 7 (l) and (p), the notable increase in the pH value in figure 8 and Mg^{2+} ion concentration in the culture medium in figure 9, and the H_2 gas evolution. The cell death was caused by the H_2 gas, Mg^{2+} and OH^- ion release (the pH increase), which permeated through the coating layer and cracks [33]. Furthermore, it is noted that in the outermost layer of the pH 10.2 coating, the needle-shaped HAp crystals possessed a diameter of tens of nanometers with a very sharp tip [17]. It is proved that the sharp-tip nanotopography was harmful to the elongation of the cells and led to a decreased in the cell density and cell shrinkage [38]. Moreover, the surface containing high-density nano-particles caused a drastic decrease in the number of the osteoblasts [39]. Hence, the morphology of the pH 10.2 coating also plays an essential role on the low cell proliferation on this sample.

In addition, compared the cell density and corrosion among the samples, it is believed that the coating morphology is more dominant for cell adhesion and proliferation than the corrosion protectiveness of the coating.

4.2. In vivo degradation behavior of subcutaneously implanted samples

The degradation process of an implanted material depends upon the host response which is controlled by the surface properties of the material, resulting in the latter changes in its structure, mechanical properties and performance [20], [40]. Based on the standing-out results of the sample coated at pH 7.8 shown in the cell culture test with the best cellular biocompatibility and corrosion resistance, this sample was selected to be implanted subcutaneously in the rabbit body. The uncoated sample was also implanted to compare. This implantation in rabbits aimed to give an insight into the feasibility and degradation behavior of the ZK60 alloy coated at the optimum condition of pH 7.8. However, the *in vivo* behavior of this sample in hard tissues should be further examined even though this study pointed out that it showed good *in vitro* biocompatibility with the osteoblastic cells.

In the host response, the capsule tissue is created by the combination of macrophages, fibroblasts and a build-up extracellular matrix [41]. The formation of the capsule around the implant, or the fibrous encapsulation shown in Figure 10, separates the implant from the surrounding tissues and body fluid. The isolation of the fibrous capsule and the gas cavities, together with the formation of corrosion products as in figure 12, slowed down the corrosion of the implant samples [42]. The degradation of the implanted material is believed to be caused mainly by macrophages [29], [43]. When macrophages adhere to the surface of the implant, they secrete mediators of degradation (reactive oxygen and nitrogen species, degradative enzymes and acid hydrolases) into a privileged microenvironment which was induced between the cell membrane and the surface of the implant [44]. The local corrosion, typically pitting, occurred under this privileged microenvironment. It is stated that the local corrosion occurred in narrow regions with fixed positions of micro-Mg anodes and cathodes (such as impurities, second phases or intermetallic compounds) due to the limited diffusion of the body fluid, which was caused by the adhesion of human immune cells [45]. Therefore, Mg anodes were corroded vertically *in vivo* and caused deep pitting regions shown in figures 11 and 12. Xia et al. proved that HAp was degraded by macrophages [46]. Moreover, the HAp crystals formed by the employed chemical conversion method exhibit a nonstoichiometric composition with the incorporation of CO_3 in PO_4 sites and Na and/or Mg in Ca sites [47]. Therefore, HAp crystals were degraded *in vivo*, leading to the thinner and shorter crystals after four weeks of implantation, as in figure 13. Hiromoto *et al.* also reported that the HAp coating was dissolved locally during the subcutaneous implantation in transgenic mice [45].

Hydrogen gas evolution is an inevitable consequence as the samples were degraded. The initial hydrogen evolution led to the formation of gas cavities. It is reported that the gas cavities caused a decrease in the survival rate of rats [48]. However, in this study, the cavities showed no effects on the survival rate of the rabbits until twelve weeks post-surgery, except for the swelling at the implantation site and discomfort to the rabbits in their daily activities. The volume of hydrogen gas can be reduced because hydrogen gas saturates the adjacent tissues, exchanges with dissolved gasses (nitrogen, oxygen and carbon dioxide) from the adjacent tissues and blood vessels, and diffuses through the skin [49]. While hydrogen gas was exchanged from the inside to the outside of the gas cavities, the samples were continuing to be corroded and further hydrogen gas was evolved. In figure 10 (a) and (b), after four weeks of implantation, gas cavities were observed obviously in both types of the implanted samples although the HAp coating is expected to delay the initial corrosion of the coated sample. The corrosion of the uncoated sample was occurred immediately after implantation, whereas the corrosion of the coated sample was supposed to initiate from the defects of the HAp coating which either already exists or caused during the implantation process, in addition to the activities of the immune cells. In figure 10 (c) and (d), the difference in the size

of the gas cavities between the uncoated and coated samples was noticeable after twelve weeks of implantation. The significant reduction of gas around the coated sample indicates that the corrosion rate of this sample was delayed remarkably and lower than the exchange rate of hydrogen gas. This decrease in the corrosion rate is attributed to the corrosion protection from the remained HAp coating and the corrosion product layer. $Mg(OH)_2$ can be absorbed poorly in the digestive system and degraded by the acid in form of H_2O_2 released by neutrophils and macrophages [48]. It means that further corrosion of the coated sample can take place.

Hence, with the preferred surface conditions, higher corrosion resistance and a notable reduction of gas cavities at the implantation site, the sample coated at pH 7.8 was presumed to reduce the inflammation level and limit the clinical concerns caused by the high corrosion rate of the uncoated ZK60. However, further investigation related to foreign body reaction should be studied.

5. Conclusion

In vitro biocompatibility was studied on several calcium phosphate coatings formed on ZK60 alloy using MC3T3-E1 pre-osteoblasts. The type, surface morphology and corrosion protectiveness of the coatings governed the morphology, adhesion and proliferation of the cells. Among those surface factors, the morphology of the coating is more dominant for cell adhesion and proliferation than its corrosion protectiveness. Compared with the seeding density, the cell density increased about twice on the samples coated at pH 6.5 and 7.8, whereas decreased to about 26.4% on the sample coated at pH 10.2 after 72h. The cells were more elongated and had larger nucleus area on the pH 7.8 coating than on the pH 6.5 coating but shrunk severely on the pH 10.2 coating. The sample coated at pH 7.8 showed the best cellular biocompatibility.

In vivo degradation behavior of the samples that were uncoated and coated at pH 7.8 was studied by the subcutaneous implantation in rabbits. Gas cavities were formed around both types of the samples due to their corrosion after four weeks of implantation. Compared with the uncoated sample, the volume of gas cavities reduced significantly around the sample coated at pH 7.8 after twelve weeks due to its higher corrosion resistance. Pitting was the main corrosion mechanism that occurred in the rabbit body. The HAp coating was also degraded during implantation, shown by the sparse distribution of the thinned and shortened HAp crystals.

In general, the sample coated at pH 7.8 showed the best cellular biocompatibility and improved notably the corrosion resistance of ZK60 alloy both *in vitro* and *in vivo*. Therefore, ZK60 alloy coated at 7.8 can be a degradable implant for clinical use.

Declaration of interests

The authors declare that they have no known competing financial interests or personal relationships that could have appeared to influence the work reported in this paper.

Reference

[1] M. Niinomi, M. Nakai, J. Hieda, Development of new metallic alloys for biomedical applications, Acta Biomaterialia. 8 (2012) 3888–3903. https://doi.org/10.1016/j.actbio.2012.06.037.

[2] S. Kamrani, C. Fleck, Biodegradable magnesium alloys as temporary orthopaedic implants: a review, Biometals. 32 (2019) 185–193. https://doi.org/10.1007/s10534-019-00170-y.

[3] X.N. Gu, N. Li, Y.F. Zheng, L. Ruan, In vitro degradation performance and biological response of a Mg–Zn–Zr alloy, Materials Science and Engineering: B. 176 (2011) 1778–1784. https://doi.org/10.1016/j.mseb.2011.05.032.

[4] Z.G. Huan, M.A. Leeflang, J. Zhou, L.E. Fratila-Apachitei, J. Duszczyk, In vitro degradation behavior and cytocompatibility of Mg–Zn–Zr alloys, J Mater Sci: Mater Med. 21 (2010) 2623–2635. https://doi.org/10.1007/s10856-010-4111-8.

[5] J. Chen, L. Tan, K. Yang, Effect of heat treatment on mechanical and biodegradable properties of an extruded ZK60 alloy, Bioactive Materials. 2 (2017) 19–26. https://doi.org/10.1016/j.bioactmat.2016.12.002.

[6] G. Mani, M.D. Feldman, D. Patel, C.M. Agrawal, Coronary stents: A materials perspective, Biomaterials. 28 (2007) 1689–1710. https://doi.org/10.1016/j.biomaterials.2006.11.042.

[7] G. Song, Control of biodegradation of biocompatable magnesium alloys, Corrosion Science. 49 (2007) 1696–1701. https://doi.org/10.1016/j.corsci.2007.01.001.

[8] D. Zhao, F. Witte, F. Lu, J. Wang, J. Li, L. Qin, Current status on clinical applications of magnesium-based orthopaedic implants: A review from clinical translational perspective, Biomaterials. 112 (2017) 287–302. https://doi.org/10.1016/j.biomaterials.2016.10.017.

[9] R. Radha, D. Sreekanth, Insight of magnesium alloys and composites for orthopedic implant applications – a review, Journal of Magnesium and Alloys. 5 (2017) 286–312. https://doi.org/10.1016/j.jma.2017.08.003.

[10] H. Zhou, L. Yang, U. Gbureck, S.B. Bhaduri, P. Sikder, Monetite, an important calcium phosphate compound–Its synthesis, properties and applications in orthopedics, Acta Biomaterialia. 127 (2021) 41–55. https://doi.org/10.1016/j.actbio.2021.03.050.

[11] X.-J. Ji, L. Gao, J.-C. Liu, R.-Z. Jiang, F.-Y. Sun, L.-Y. Cui, S.-Q. Li, K.-Q. Zhi, R.-C. Zeng, Z.-L. Wang, Corrosion resistance and antibacterial activity of hydroxyapatite coating induced by ciprofloxacin-loaded polymeric multilayers on magnesium alloy, Progress in Organic Coatings. 135 (2019) 465–474. https://doi.org/10.1016/j.porgcoat.2019.06.048.

[12] W.-H. Song, H.S. Ryu, S.-H. Hong, Antibacterial properties of Ag (or Pt)-containing calcium phosphate coatings formed by micro-arc oxidation, Journal of Biomedical Materials Research Part A. 88A (2009) 246–254. https://doi.org/10.1002/jbm.a.31877.

[13] Y. Ando, H. Miyamoto, I. Noda, N. Sakurai, T. Akiyama, Y. Yonekura, T. Shimazaki, M. Miyazaki, M. Mawatari, T. Hotokebuchi, Calcium phosphate coating containing silver shows high antibacterial

activity and low cytotoxicity and inhibits bacterial adhesion, Materials Science and Engineering: C. 30 (2010) 175–180. https://doi.org/10.1016/j.msec.2009.09.015.

[14] M. Kazemzadeh-Narbat, J. Kindrachuk, K. Duan, H. Jenssen, R.E.W. Hancock, R. Wang, Antimicrobial peptides on calcium phosphate-coated titanium for the prevention of implant-associated infections, Biomaterials. 31 (2010) 9519–9526. https://doi.org/10.1016/j.biomaterials.2010.08.035.

[15] G.Y. Liu, J. Hu, Z.K. Ding, C. Wang, Bioactive calcium phosphate coating formed on micro-arc oxidized magnesium by chemical deposition, Applied Surface Science. 257 (2011) 2051–2057. https://doi.org/10.1016/j.apsusc.2010.09.050.

[16] S. Hiromoto, A. Yamamoto, High corrosion resistance of magnesium coated with hydroxyapatite directly synthesized in an aqueous solution, Electrochimica Acta. 54 (2009) 7085–7093. https://doi.org/10.1016/j.electacta.2009.07.033.

[17] M. Tomozawa, S. Hiromoto, Microstructure of hydroxyapatite- and octacalcium phosphate-coatings formed on magnesium by a hydrothermal treatment at various pH values, Acta Materialia. 59 (2011) 355–363. https://doi.org/10.1016/j.actamat.2010.09.041.

[18] C. Knabe, R. Gildenhaar, G. Berger, W. Ostapowicz, R. Fitzner, R.J. Radlanski, U. Gross, Morphological evaluation of osteoblasts cultured on different calcium phosphate ceramics, Biomaterials. 18 (1997) 1339–1347. https://doi.org/10.1016/S0142-9612(97)00078-1.

[19] M. Kamitakahara, Y. Uno, K. Ioku, Behavior of osteoblast-like cells on calcium-deficient hydroxyapatite ceramics composed of particles with different shapes and sizes, J Mater Sci: Mater Med. 25 (2014) 239–245. https://doi.org/10.1007/s10856-013-5063-6.

[20] K. Anselme, M. Bigerelle, Role of materials surface topography on mammalian cell response, International Materials Reviews. 56 (2011) 243–266. https://doi.org/10.1179/1743280411Y.0000000001.

[21] S. Samavedi, A.R. Whittington, A.S. Goldstein, Calcium phosphate ceramics in bone tissue engineering: A review of properties and their influence on cell behavior, Acta Biomaterialia. 9 (2013) 8037–8045. https://doi.org/10.1016/j.actbio.2013.06.014.

[22] Y. Fujishiro, T. Sato, A. Okuwaki, Coating of hydroxyapatite on metal plates using thermal dissociation of calcium-EDTA chelate in phosphate solutions under hydrothermal conditions, J Mater Sci: Mater Med. 6 (1995) 172–176. https://doi.org/10.1007/BF00120295.

[23] S. Hiromoto, M. Tomozawa, Hydroxyapatite coating of AZ31 magnesium alloy by a solution treatment and its corrosion behavior in NaCl solution, Surface and Coatings Technology. 205 (2011) 4711–4719. https://doi.org/10.1016/j.surfcoat.2011.04.036.

[24] L.T. Trang, N. Quang Cao, S. Hiromoto, M. O, E. Kobayashi, Formation and corrosion behavior of calcium phosphate coating layers on ZK60 alloy coated at various pH conditions by chemical conversion method, Surface and Coatings Technology. 444 (2022) 128639. https://doi.org/10.1016/j.surfcoat.2022.128639.

[25] C.K. Mann, J.H. Yoe, Spectrophotometric Determination of Magnesium with Sodium 1-Azo-2-hydroxy-3-(2,4-dimethylcarboxanilido)-naphthalene-1′-(2-hydroxybenzene-5-sulfonate), Anal. Chem. 28 (1956) 202–205. https://doi.org/10.1021/ac60110a016.

[26] D. Ratge, K.P. Kohse, H. Wisser, Measurement of magnesium in serum and urine with a random access analyzer by use of a modified xylidyl blue-1 procedure, Clinica Chimica Acta. 159 (1986) 197–203. https://doi.org/10.1016/0009-8981(86)90052-5.

[27] M. Tomozawa, S. Hiromoto, Growth mechanism of hydroxyapatite-coatings formed on pure magnesium and corrosion behavior of the coated magnesium, Applied Surface Science. 257 (2011) 8253–8257. https://doi.org/10.1016/j.apsusc.2011.04.087.

[28] P. Jevtić, L.J. Edens, L.D. Vuković, D.L. Levy, Sizing and shaping the nucleus: mechanisms and significance, Current Opinion in Cell Biology. 28 (2014) 16–27. https://doi.org/10.1016/j.ceb.2014.01.003.

[29] J. Zhang, S. Hiromoto, T. Yamazaki, J. Niu, H. Huang, G. Jia, H. Li, W. Ding, G. Yuan, Effect of macrophages on in vitro corrosion behavior of magnesium alloy, Journal of Biomedical Materials Research Part A. 104 (2016) 2476–2487. https://doi.org/10.1002/jbm.a.35788.

[30] C.L. Liu, Y.J. Wang, R.C. Zeng, X.M. Zhang, W.J. Huang, P.K. Chu, In vitro corrosion degradation behaviour of Mg–Ca alloy in the presence of albumin, Corrosion Science. 52 (2010) 3341–3347. https://doi.org/10.1016/j.corsci.2010.06.003.

[31] H. Rubin, Magnesium: The missing element in molecular views of cell proliferation control, BioEssays. 27 (2005) 311–320. https://doi.org/10.1002/bies.20183.

[32] F. Seuss, S. Seuss, M.C. Turhan, B. Fabry, S. Virtanen, Corrosion of Mg alloy AZ91D in the presence of living cells, Journal of Biomedical Materials Research Part B: Applied Biomaterials. 99B (2011) 276–281. https://doi.org/10.1002/jbm.b.31896.

[33] S. Hiromoto, T. Yamazaki, Micromorphological effect of calcium phosphate coating on compatibility of magnesium alloy with osteoblast, Science and Technology of Advanced Materials. 18 (2017) 96–109. https://doi.org/10.1080/14686996.2016.1266238.

[34] A.L. Boskey, M. Maresca, W. Ullrich, S.B. Doty, W.T. Butler, C.W. Prince, Osteopontin-hydroxyapatite interactions in vitro: inhibition of hydroxyapatite formation and growth in a gelatin-gel, Bone and Mineral. 22 (1993) 147–159. https://doi.org/10.1016/S0169-6009(08)80225-5.

[35] B. Feng, J. Weng, B.C. Yang, S.X. Qu, X.D. Zhang, Characterization of titanium surfaces with calcium and phosphate and osteoblast adhesion, Biomaterials. 25 (2004) 3421–3428. https://doi.org/10.1016/j.biomaterials.2003.10.044.

[36] C. Combes, C. Rey, Adsorption of proteins and calcium phosphate materials bioactivity, Biomaterials. 23 (2002) 2817–2823. https://doi.org/10.1016/S0142-9612(02)00073-X.

[37] L. Wang, G.H. Nancollas, Calcium Orthophosphates: Crystallization and Dissolution, Chem. Rev. 108 (2008) 4628–4669. https://doi.org/10.1021/cr0782574.

[38] C.-H. Choi, S.H. Hagvall, B.M. Wu, J.C.Y. Dunn, R.E. Beygui, C.-J. "CJ" Kim, Cell interaction with three-dimensional sharp-tip nanotopography, Biomaterials. 28 (2007) 1672–1679. https://doi.org/10.1016/j.biomaterials.2006.11.031.

[39] T.P. Kunzler, C. Huwiler, T. Drobek, J. Vörös, N.D. Spencer, Systematic study of osteoblast response to nanotopography by means of nanoparticle-density gradients, Biomaterials. 28 (2007) 5000–5006. https://doi.org/10.1016/j.biomaterials.2007.08.009.

[40] C. Li, C. Guo, V. Fitzpatrick, A. Ibrahim, M.J. Zwierstra, P. Hanna, A. Lechtig, A. Nazarian, S.J. Lin, D.L. Kaplan, Design of biodegradable, implantable devices towards clinical translation, Nat Rev Mater. 5 (2020) 61–81. https://doi.org/10.1038/s41578-019-0150-z.

[41] A. Carnicer-Lombarte, S.-T. Chen, G.G. Malliaras, D.G. Barone, Foreign Body Reaction to Implanted Biomaterials and Its Impact in Nerve Neuroprosthetics, Frontiers in Bioengineering and Biotechnology. 9 (2021). https://doi.org/10.3389/fbioe.2021.622524.

[42] N.I. Zainal Abidin, B. Rolfe, H. Owen, J. Malisano, D. Martin, J. Hofstetter, P.J. Uggowitzer, A. Atrens, The in vivo and in vitro corrosion of high-purity magnesium and magnesium alloys WZ21 and AZ91, Corrosion Science. 75 (2013) 354–366. https://doi.org/10.1016/j.corsci.2013.06.019.

[43] C. Chu, L. Liu, S. Rung, Y. Wang, Y. Ma, C. Hu, X. Zhao, Y. Man, Y. Qu, Modulation of foreign body reaction and macrophage phenotypes concerning microenvironment, Journal of Biomedical Materials Research Part A. 108 (2020) 127–135. https://doi.org/10.1002/jbm.a.36798.

[44] P.M. Henson, The Immunologic Release of Constituents from Neutrophil Leukocytes: II. Mechanisms of Release During Phagocytosis, and Adherence to Nonphagocytosable Surfaces, The Journal of Immunology. 107 (1971) 1547–1557. https://www.jimmunol.org/content/107/6/1547 (accessed June 10, 2022).

[45] S. Hiromoto, M. Inoue, T. Taguchi, M. Yamane, N. Ohtsu, In vitro and in vivo biocompatibility and corrosion behaviour of a bioabsorbable magnesium alloy coated with octacalcium phosphate and hydroxyapatite, Acta Biomaterialia. 11 (2015) 520–530. https://doi.org/10.1016/j.actbio.2014.09.026.

[46] Z. Xia, T. Zhu, J. Du, Q. Zheng, L. Wang, S. Li, C. Chang, S. Fang, Macrophages in degradation of collagen/hydroxylapatite(CHA), beta-tricalcium phosphate ceramics (TCP) artificial bone graft: An in vivo study, Chinese Medical Journal. 107 (1994) 845–849. https://doi.org/10.5555/cmj.0366-6999.107.11.p845.01.

[47] N. Ohtsu, S. Hiromoto, M. Yamane, K. Satoh, M. Tomozawa, Chemical and crystallographic characterizations of hydroxyapatite- and octacalcium phosphate-coatings on magnesium synthesized by chemical solution deposition using XPS and XRD, Surface and Coatings Technology. 218 (2013) 114–118. https://doi.org/10.1016/j.surfcoat.2012.12.037.

[48] D. Noviana, D. Paramitha, M.F. Ulum, H. Hermawan, The effect of hydrogen gas evolution of magnesium implant on the postimplantation mortality of rats, Journal of Orthopaedic Translation. 5 (2016) 9–15. https://doi.org/10.1016/j.jot.2015.08.003.

[49] J. Kuhlmann, I. Bartsch, E. Willbold, S. Schuchardt, O. Holz, N. Hort, D. Höche, W.R. Heineman, F. Witte, Fast escape of hydrogen from gas cavities around corroding magnesium implants, Acta Biomaterialia. 9 (2013) 8714–8721. https://doi.org/10.1016/j.actbio.2012.10.008.

Figures and Captions

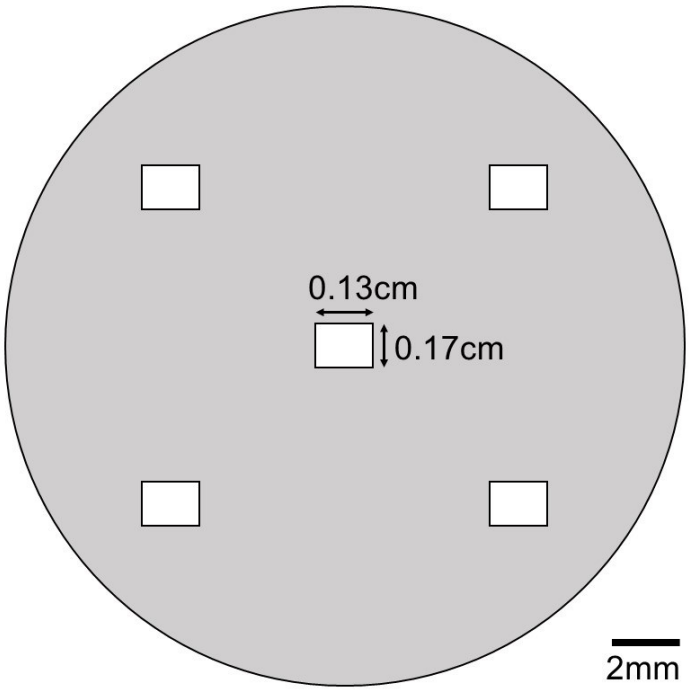

Figure 1: Five places to count cells on each sample after the cell culture test.

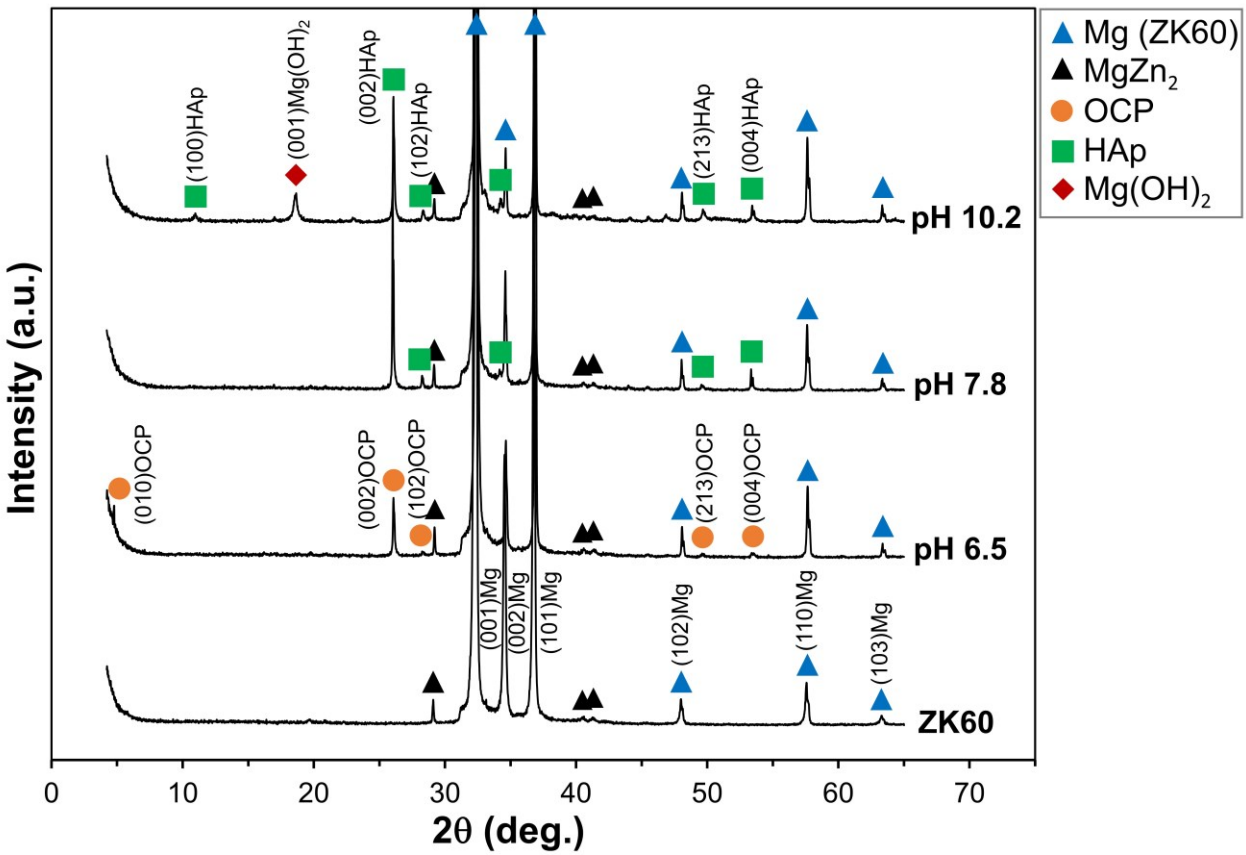

Figure 2: XRD diffraction patterns of the uncoated and coated samples [24].

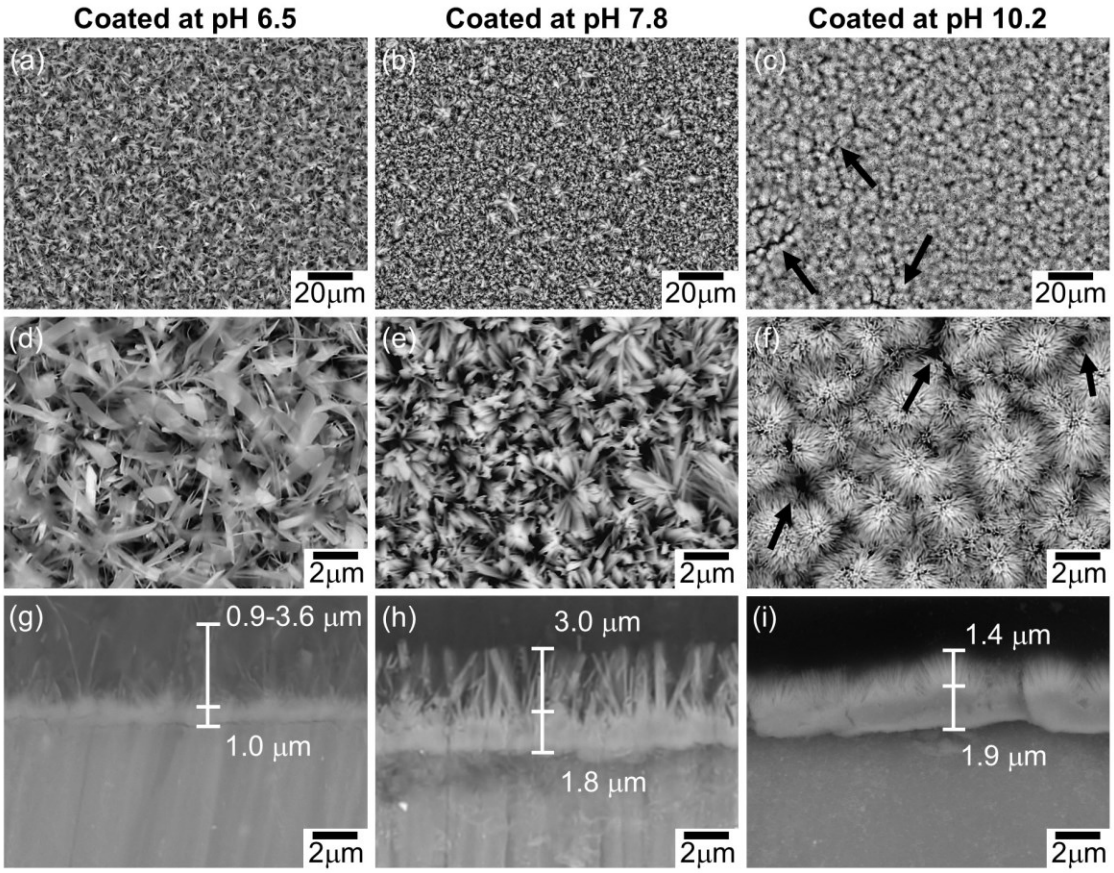

Figure 3: Surface and cross-section SEM images of the samples coated at pH 6.5 ((a), (d) and (g)), at pH 7.8 ((b), (e) and (h)) and at pH 10.2 ((c), (f) and (i)) [24].

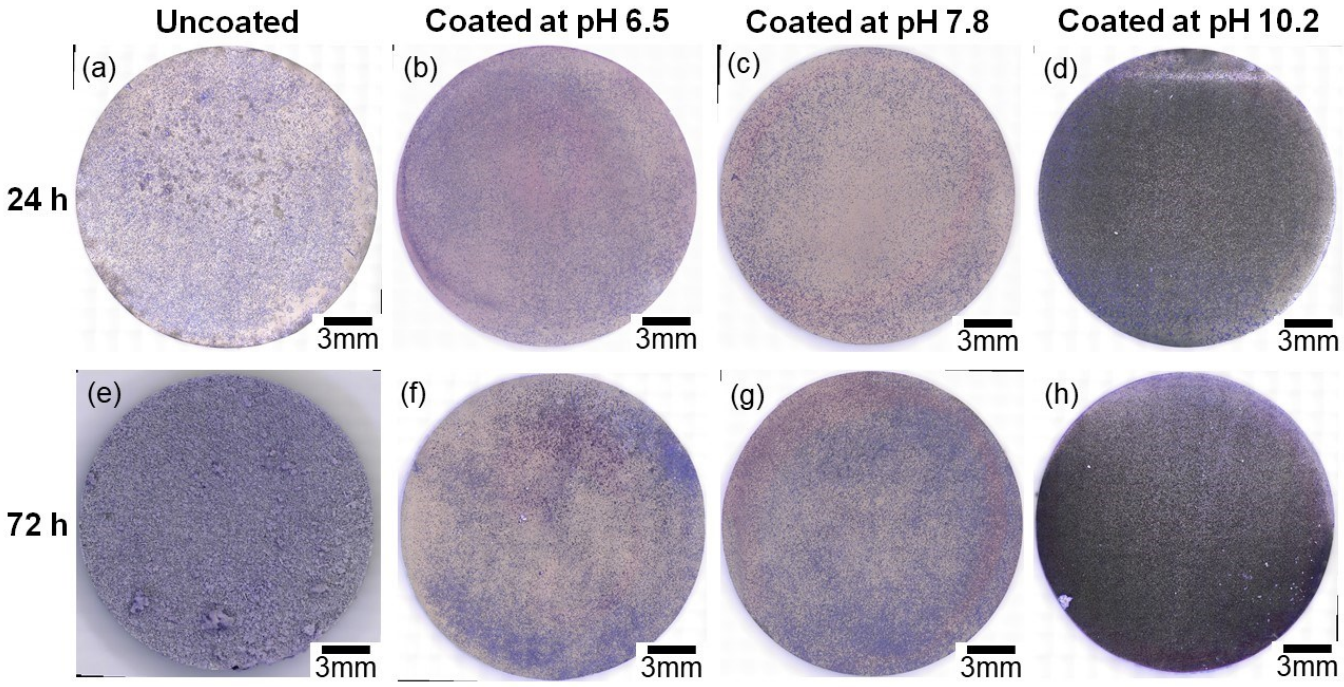

Figure 4: OM images of the samples after 24h ((a) to (d)) and 72h ((e) to (h)) of the cell culture test.

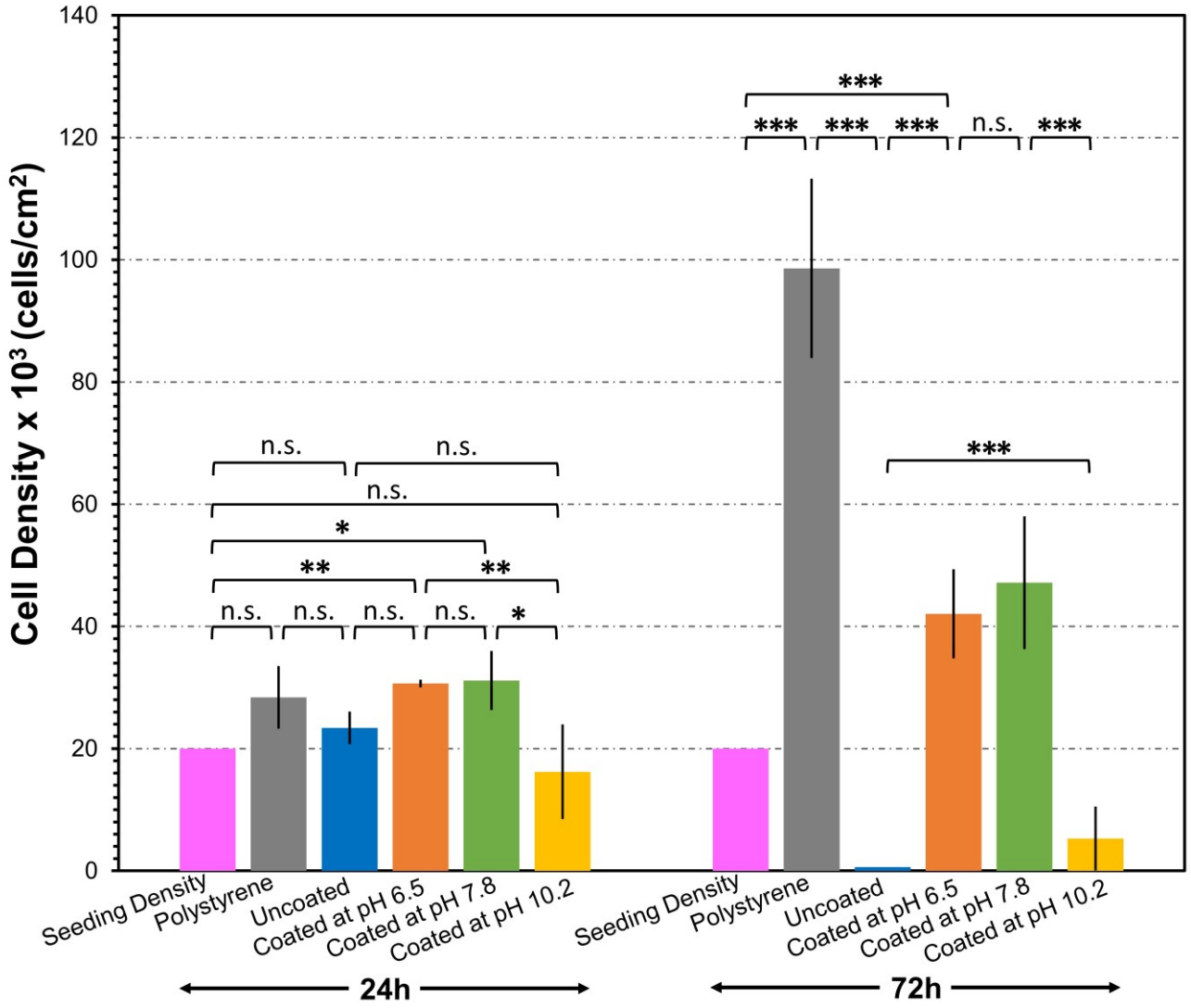

Figure 5: MC3T3-E1 cell density on different types of samples. n.s.: not significant, *: $p \leq 0.1$, **: $p \leq 0.05$, ***: $p \leq 0.001$.

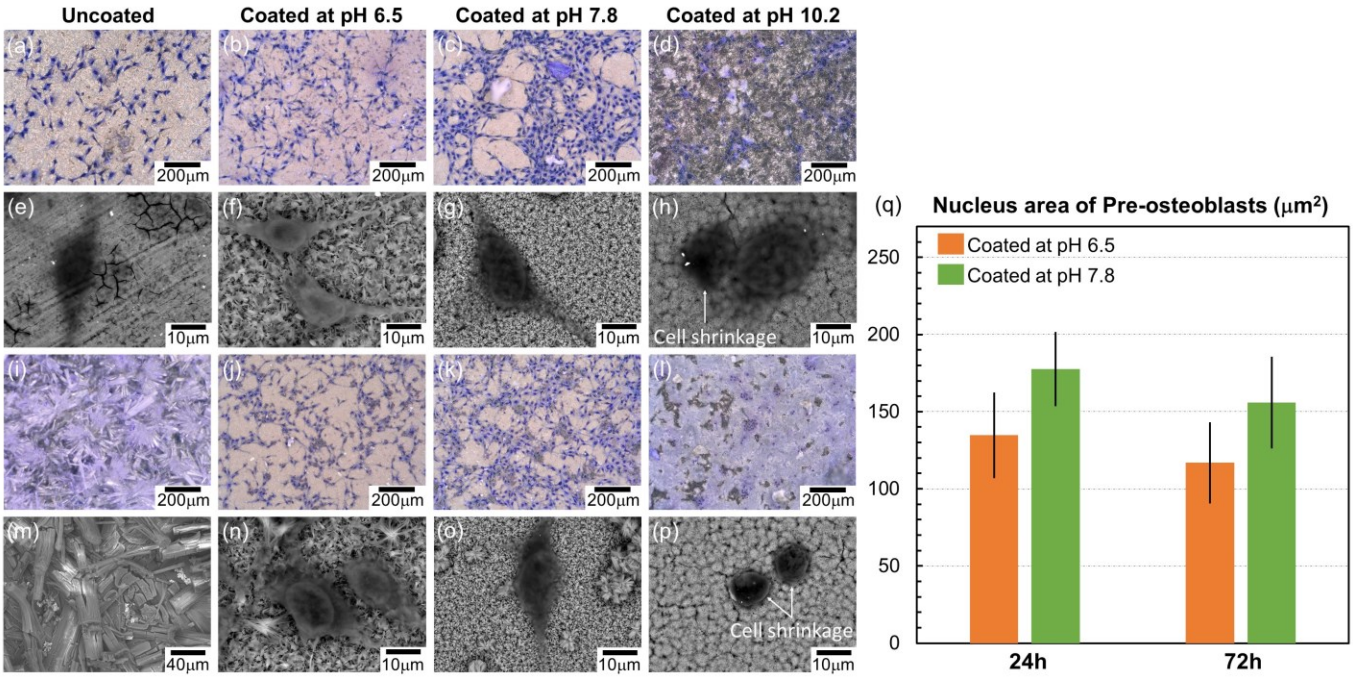

Figure 6: OM ((a) to (d) and (i) to (l)) and SEM ((e) to (h) and (m) to (p)) images of cell morphology on the samples uncoated ((a), (e), (i) and (m)), coated at pH 6.5 ((b), (f), (j) and (n)), coated at pH 7.8 ((c), (g), (k) and (o)) and coated at pH 10.2 ((d), (h), (l) and (p)) after 24h ((a) to (h)) and after 72h ((i) to (p)). (q) the nucleus area of the cells adhered on the sample coated at pH 6.5 and 7.8 after 24h and 72h.

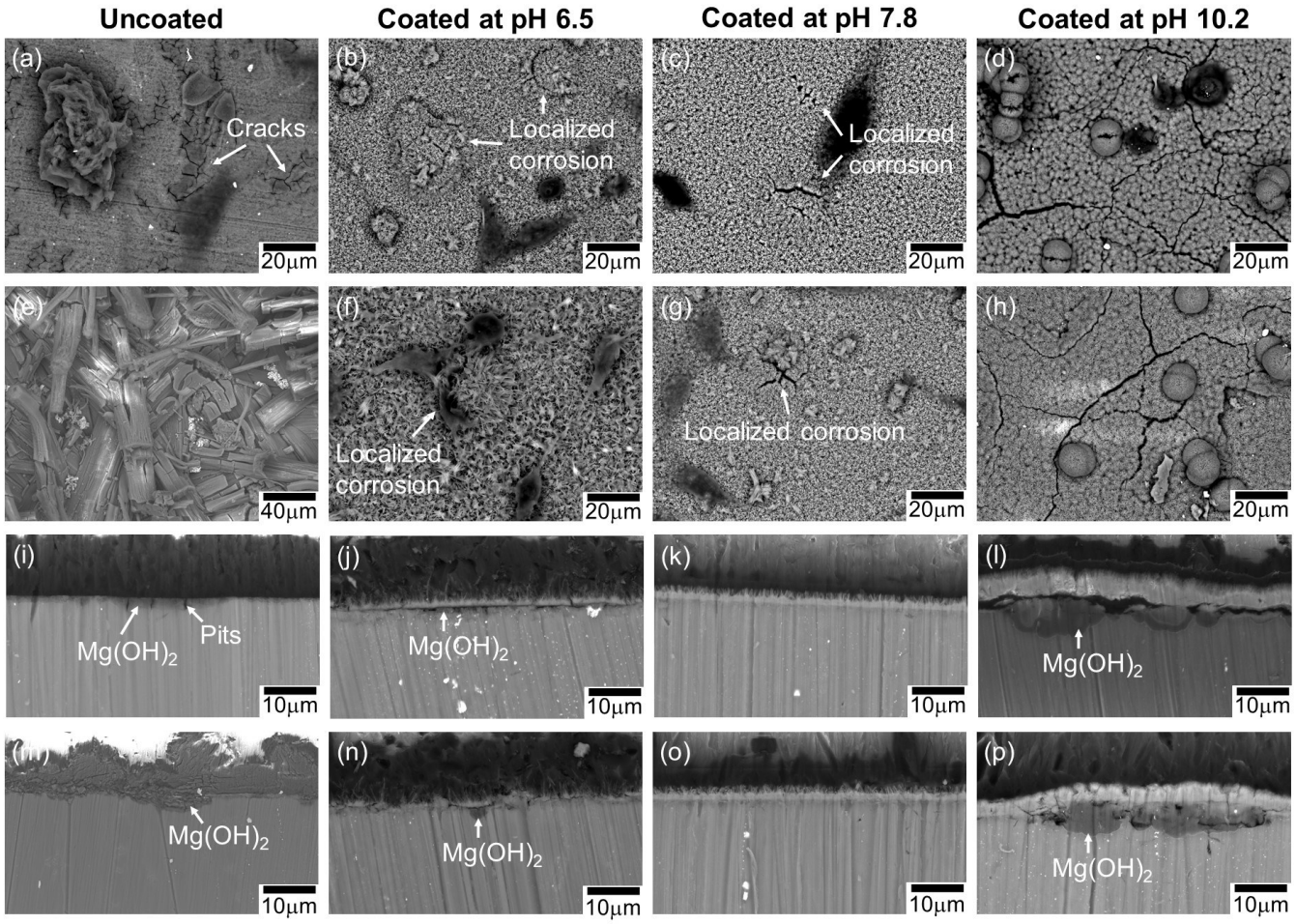

Figure 7: Surface ((a) to (h)) and cross-sectional ((i) to (p)) backscattered SEM micrographs of all the samples uncoated ((a), (e), (i) and (m)), coated at pH 6.5 ((b), (f), (j) and (n)), coated at pH 7.8 ((c), (g), (k) and (o)) and coated at pH 10.2 (d), (h), (l) and (p)) after 24h ((a) to (d) and (i) to (l)) and 72h ((e) to (h), (m) to (p)).

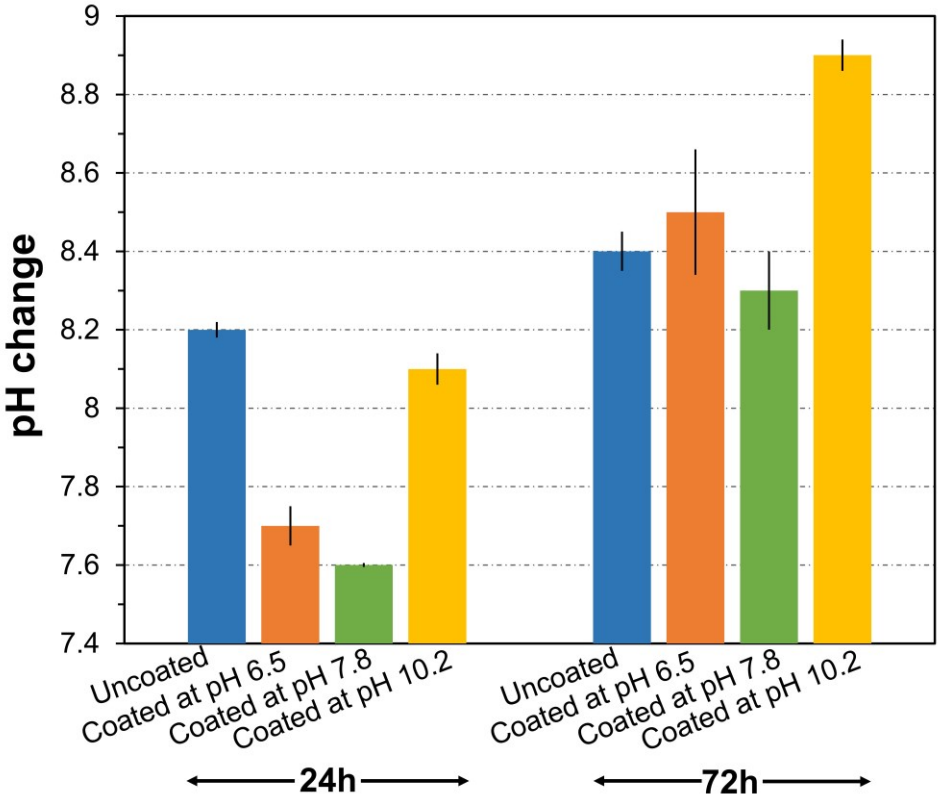

Figure 8: pH change of the medium for all the samples after 24 h and 72h culture.

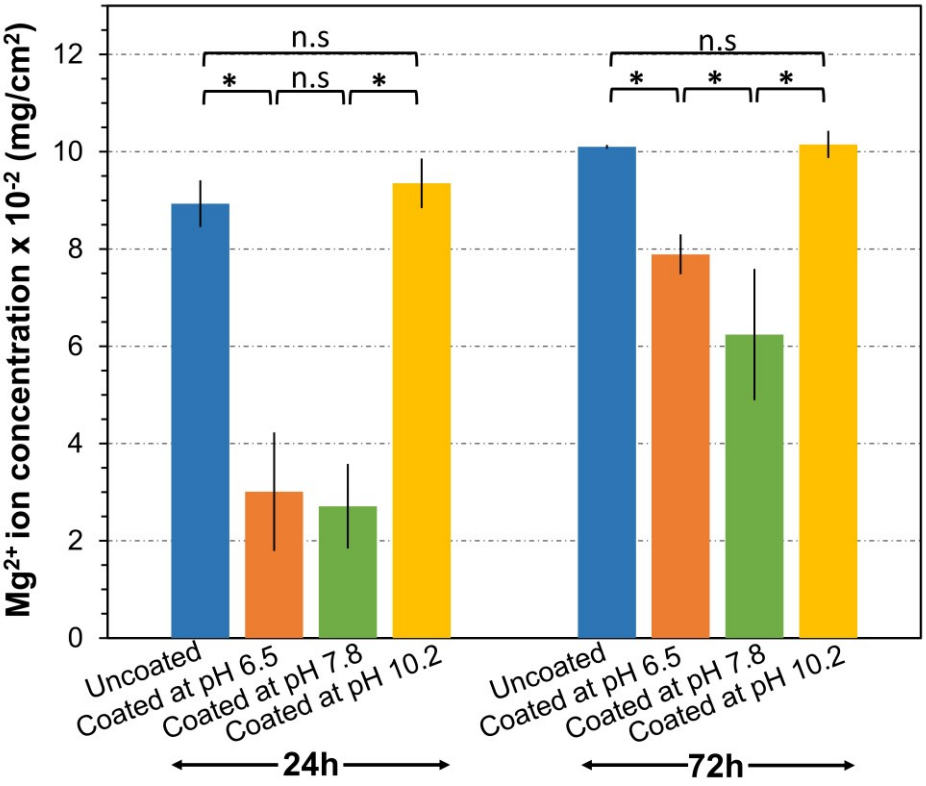

Figure 9: Mg^{2+} ion concentration of the medium for all the samples after 24h and 72h culture. n.s.: not significant, *: $p \leq 0.05$.

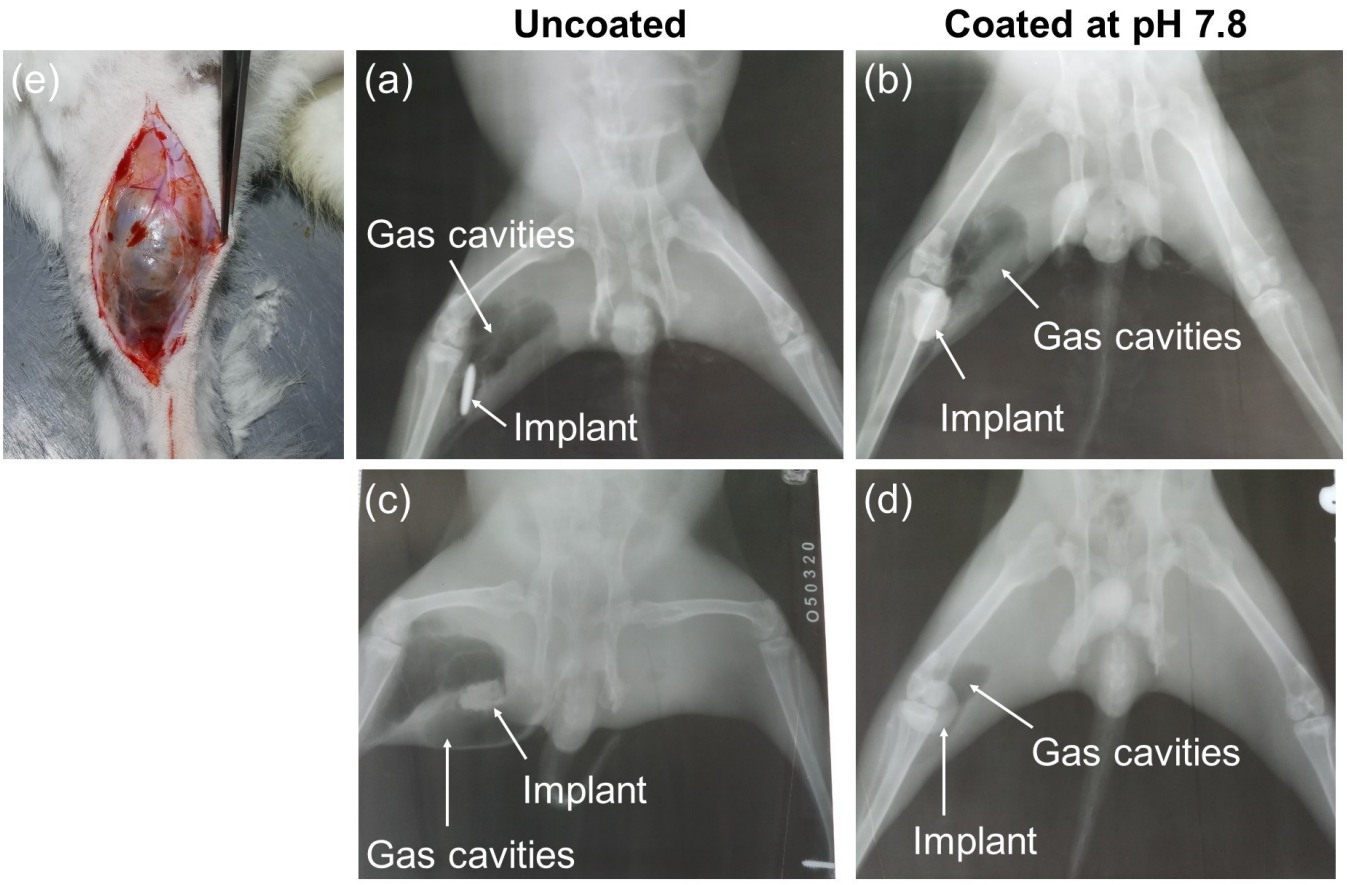

Figure 10: Radiographs of the samples: uncoated ((a) and (c)) and coated at pH 7.8 ((b) and (d)) at four weeks ((a) and (b)) and twelve weeks ((c) and (d)) post-surgery. Subcutaneous appearance of gas cavity at the implantation site of the uncoated sample at four weeks post-surgery (e).

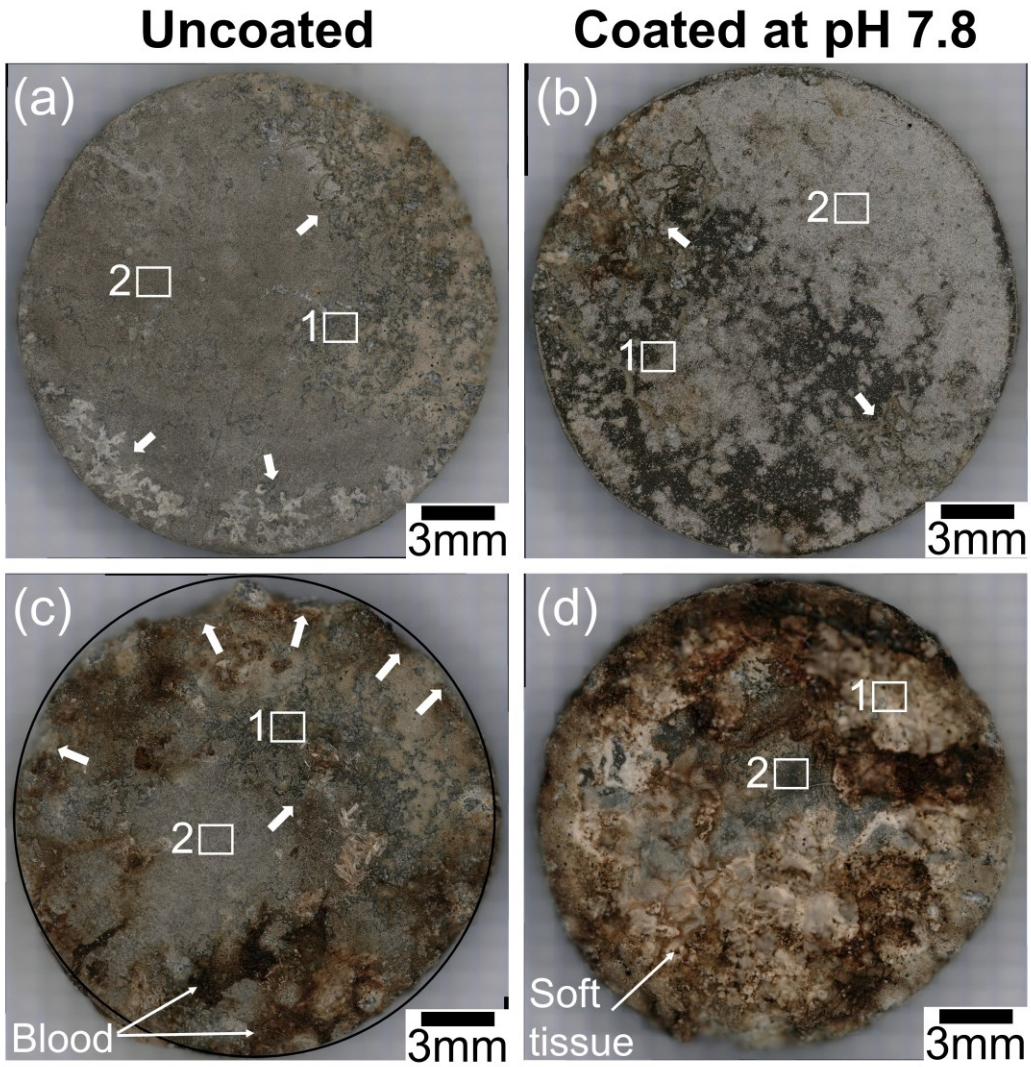

Figure 11: Microscopy images of the sample: uncoated ((a) and (c)) and coated at pH 7.8 ((b) and (d)) at four weeks ((a) and (b)) and twelve weeks ((c) and (d)) post-surgery. White arrows indicate the visible corrosion areas. The black circle corresponds to the original shape of the uncoated sample before implantation. White squares indicate the areas which are subsequently analyzed by SEM.

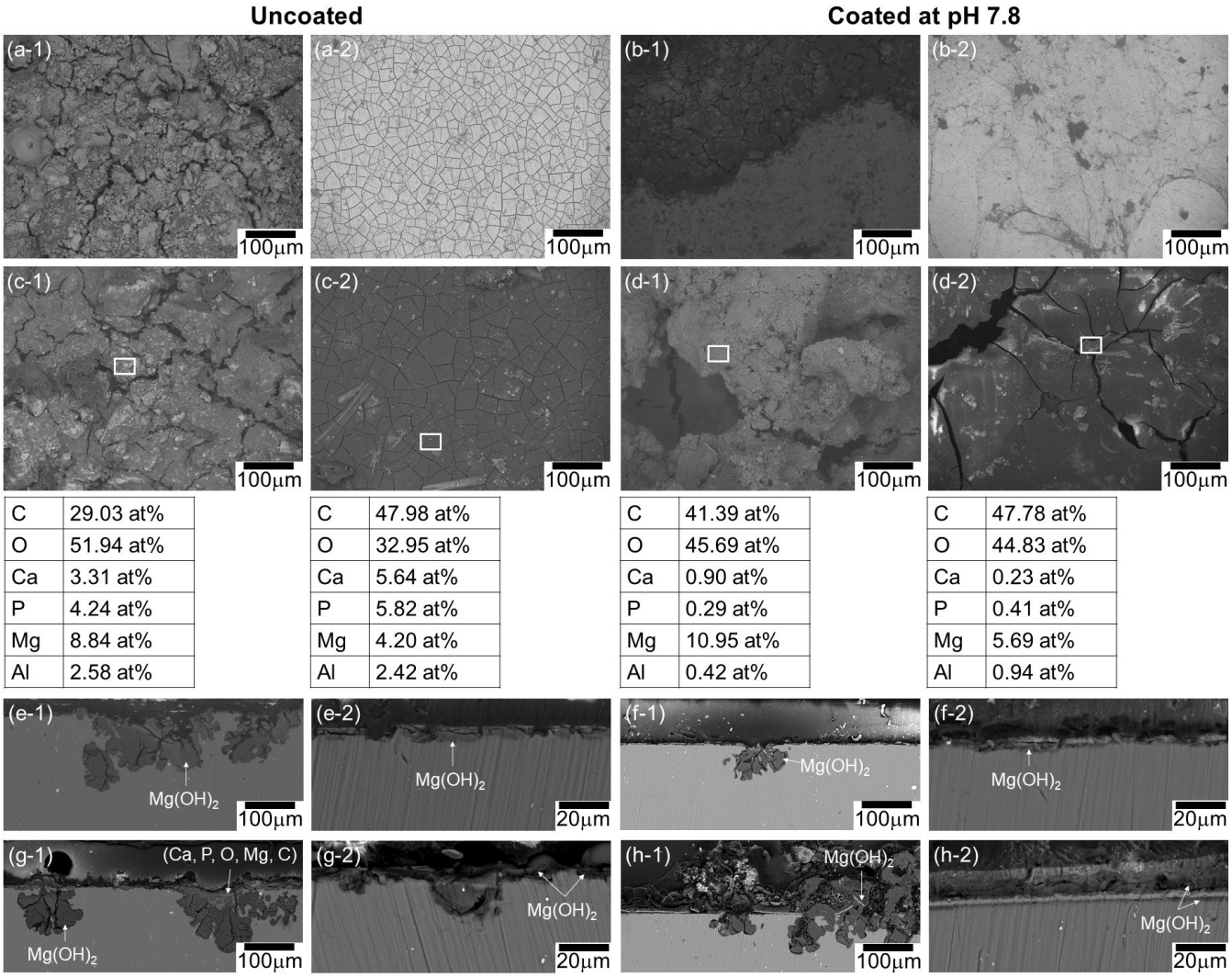

Figure 12: Surface and cross-sectional backscattered SEM images of the sample uncoated ((a), (c), (e) and (g)) and coated at pH 7.8 ((b), (d), (f) and (h)) at four weeks ((a) to (d)) and twelve weeks ((e) to (h)) post-surgery.

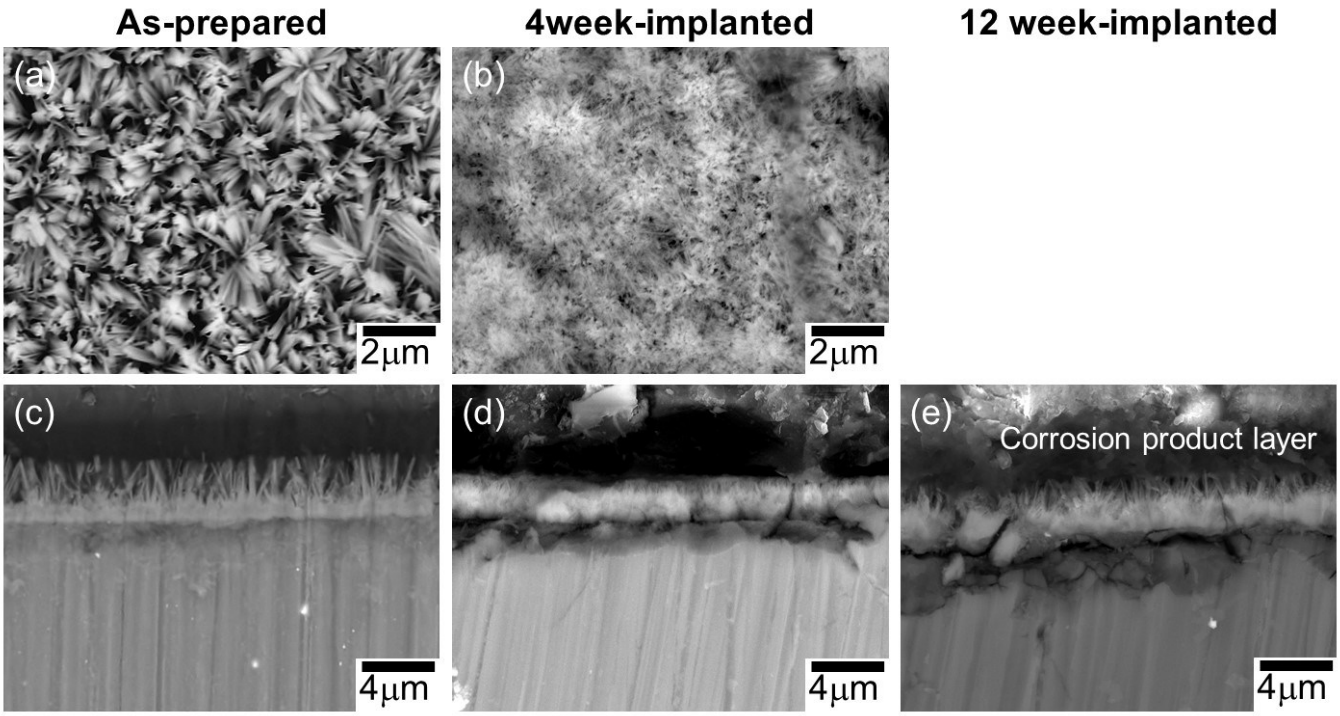

Figure 13: Change of the HAp coating formed at pH 7.8 during implantation: the as-prepared coating ((a) and (c)), the coating after four weeks ((b) and (d)) and twelve weeks (e) of implantation.